
deadtrees.earth-aerial: A Multi-Resolution Aerial Image Dataset for Tree Cover and Mortality Detection

Ayushi Sharma^{1,2} Clemens Mosig³ Lukas Drees² Salim Soltani¹
Janusch Vajna-Jehle¹ Aaron Sheppard¹ Belqis Ahmadi¹ Jonathan Schmid¹
Paul Neumeier¹ Nathan Jacobs⁴ Jan Dirk Wegner² Teja Kattenborn¹

¹Chair of Sensor-based Geoinformatics, University of Freiburg, Germany

²EcoVision Lab, DM3L, University of Zurich, Switzerland

³Institute for Earth System Science and Remote Sensing, Leipzig University, Germany

⁴Washington University, St. Louis

{ayushi.sharma, teja.kattenborn}@geosense.uni-freiburg.de
clemens.mosig@uni-leipzig.de

Abstract

Forests worldwide are increasingly threatened by climate change and disturbances such as fire, pests, and pathogens, creating an urgent need for scalable monitoring of tree cover and tree mortality. Aerial imagery from drones and aircraft is a key data source for detailed and large-scale mapping of tree crowns and mortality. However, related progress is limited by the lack of globally representative, harmonized datasets for joint segmentation of tree cover and mortality. We introduce two novel, open, machine-learning-ready datasets to enable joint segmentation of tree cover and tree mortality from centimeter-scale aerial imagery for the first time at global scales. With DTE-aerial-train, we provide a training dataset comprising 385K image patches of size 1024×1024 pixels, with resolutions ranging from 2.5 to 20 cm. It includes multi-class expert-annotated and -audited pseudo-labels for tree cover and mortality. With DTE-aerial-bench, we provide a geographically balanced benchmark test set of 25 globally distributed orthoimages totaling 525 patches with high-quality expert annotations for both tree cover and mortality. Both the training and benchmark datasets span tropical, temperate, boreal, and dryland biomes and cover a wide range of forest structures and mortality patterns. Using the benchmark test set for evaluation, we establish strong reference baselines that improve mortality segmentation across all biomes and scales with significant gains in challenging regions, such as boreal forests, where the F1 score increases from 0.40 to 0.58 with around 45% relative improvement. All data, models, and code will be publicly released under permissive open-source licenses. An interactive visualization of the benchmark dataset is available at deadtrees.earth/releases/dte-aerial-bench.

1 Introduction

The world's forests shape carbon, water, and energy fluxes while providing essential ecosystem services for human well-being, including carbon storage, biodiversity habitat, water provisioning, and protection from natural hazards [26, 12]. Under ongoing climate change, forests worldwide are increasingly exposed to rising atmospheric aridity and more frequent and prolonged droughts, leading to elevated tree mortality [14, 36, 2]. These impacts are further exacerbated by pests, pathogens, forest degradation, and wildfires [34, 28, 5]. Understanding how these stressors shape forest dynamics worldwide requires globally consistent monitoring of tree cover and mortality [19, 23].

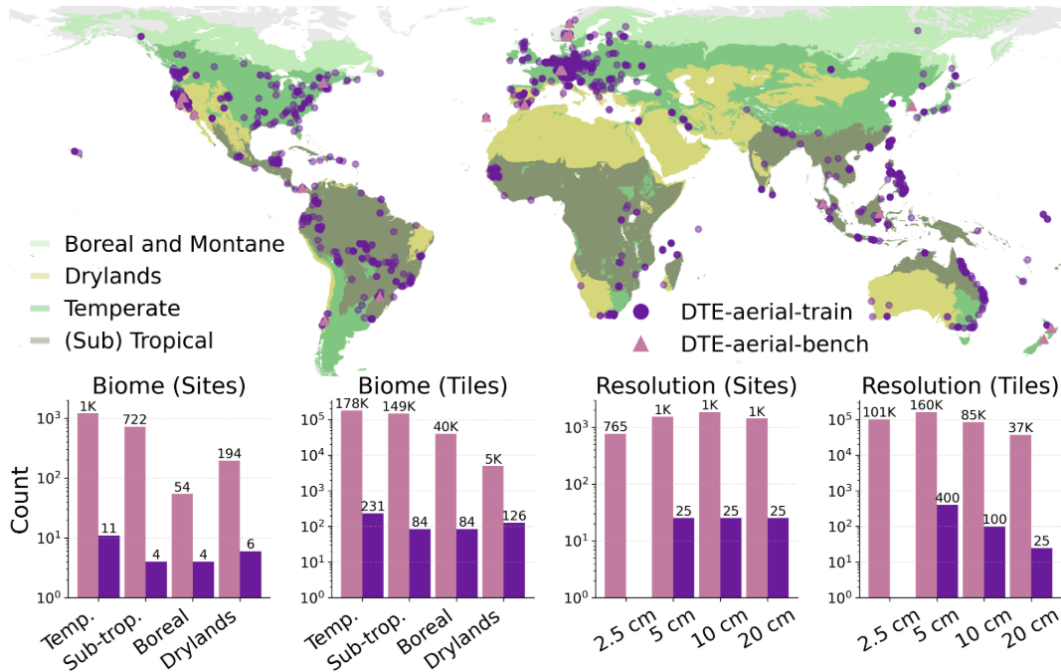


Figure 1: **Dataset overview.** (Top) Global, crowd-sourced aerial imagery from *deadtrees.earth*, representing one of the largest high-resolution collections for tree mortality. The training set spans tropical, temperate, boreal, and dryland biomes, capturing diverse canopy structures and forest conditions, while the benchmark is a curated subset emphasizing label quality. (Bottom) Distribution of sites and patches across biome groups and spatial resolutions for training and benchmark sets. Patch counts for the training set are reported in thousands to reflect scale.

Forest monitoring in this context requires accurate mapping of tree crown cover across spatial scales, as crown cover changes reflect processes such as recovery, disturbance, and degradation. In parallel, it requires precise detection of mortality in standing trees ranging from early-stage signals such as partial crown or branch dieback to fully dead standing tree crowns [23, 22].

Aerial imagery from aircraft and drones is a key data source for forest monitoring, bridging the gap between coarse-resolution satellite data and spatially limited terrestrial measurements [32]. Through national airborne campaigns, aerial imagery from aircraft has become widely available, while locally acquired drone imagery has also become abundant, emerging as a key technology for environmental monitoring [16, 22].

Airplane and drone imagery combined with modern computer vision enables scalable extraction of tree cover and tree mortality [22, 20, 32, 38]. In particular, centimeter-scale aerial RGB imagery (<10 cm) provides the spatial detail and availability needed for this task, often outperforming more complex modalities such as multispectral or hyperspectral imagery [17, 16]. While prior work has shown strong performance in both tree cover mapping and mortality detection [38, 20, 32], these tasks are typically addressed in isolation. However, joint and coherent mapping of tree cover and tree mortality is required to assess forest vitality, and is currently limited by the lack of globally consistent, ML-ready datasets with high-quality semantic annotations for both tasks [22].

Existing annotated aerial image datasets of forests do not comprehensively represent the diversity of forest types, species compositions, and functional types across global biomes [22]. Aerial images further differ substantially in spatial resolution, sensor characteristics, and illumination conditions, hindering the learning of generalizable spatial features [20, 33]. Together, these limitations constrain the development of models that generalize globally.

The lack of geographically comprehensive data limits model training and prevents effective benchmarking of methods across the world’s biomes, sensing conditions, and spatial resolutions. This issue is further compounded by the absence of standardized expert annotations, as current labels often lack

the precision required for meaningful comparison [20, 16]. As a result, the field lacks a globally representative benchmark dataset, critically limiting consistent evaluation and thereby impeding both methodological advances in the computer vision community and the selection of robust models for operational forest monitoring in applied contexts.

To address these challenges, and supported by the deadtrees.earth initiative (DTE), we make the following contributions:

- We enable standardized evaluation of tree cover and mortality segmentation across biomes and spatial resolutions using **DTE-aerial-bench**, a multi-resolution, globally representative benchmark dataset with expert-annotated, cross-scale consistent labels.
- We introduce **DTE-aerial-train**, a global, centimeter-scale, multi-resolution labeled aerial image dataset covering 2176 sites for jointly mapping tree cover and tree mortality.
- We establish baseline models for simultaneous multi-class segmentation of tree cover and mortality across diverse biomes and image resolutions, providing initial benchmarks and highlighting challenges in generalization under geographic and multi-resolution variability, as well as severe class imbalance between abundant forest cover and rare mortality instances.

Table 1: Comparison of existing open and ML-ready aerial image datasets and benchmarks for tree cover and mortality mapping. Our dataset (DTE-aerial-train) is the first centimeter-scale and multi-resolution dataset with consistent semantic segmentation annotations for both tree cover and mortality, offering global coverage across the largest quantity of high-resolution orthoimagery (sites).

Dataset	Tree Cover	Mortality	Resolution	Sites	Coverage
BAMForest [35]	✓	–	10–20 cm	4	Germany
SelvaMask [11]	✓	–	1–4 cm	3	Central/South America
Ball et al. [6]	✓	–	8–10 cm	4	Malaysia, French Guiana
OAM-TCD [38]	✓	–	10 cm	541	Global
TreeFinder [39]	–	✓	60 cm	1,000	US
Möhring et al. [20]	–	✓	1–28 cm	434	Global
FORTRESS [30]	✓	✓	1–2 cm	51	Germany
Allen et al. [3]	✓	✓	3 cm	9	Spain
DTE-aerial-train (ours)	✓	✓	2.5–20 cm	2,176	Global

2 Related work

While a range of methods, tasks and datasets have been proposed for tree and tree-mortality monitoring from aerial imagery [16], previous research showed that detecting partial crown decline and small canopy gaps requires fine-grained delineation [16, 32, 20]. In contrast, tree instance segmentation and object detection [40, 27, 9] are often ill-suited to many forest ecosystems where overlapping and interwoven crowns diffuse tree boundaries [4, 16]. We therefore focus on *semantic segmentation*, as pixel-level information and exact shapes are essential for accurately quantifying tree cover and mortality. Previous work has largely focused on either semantic segmentation of tree cover *or* tree mortality, but jointly only at national scale (Table 1). We therefore review datasets and baselines for each task separately before positioning our contributions.

Previous works on tree cover estimation Computer vision has been widely applied to tree crown segmentation from remote sensing imagery [16]. High-quality datasets and corresponding model developments are available for temperate forests [10, 35, 31] as well as tropical forests [11, 6, 37]. While these datasets have enabled strong methodological progress, they are typically developed and evaluated on geographically constrained study areas, limiting generalizability of the resulting models across the world’s forest ecosystems (Table 1).

A major step toward broader coverage was made by OAM-TCD [38], which provides tree-cover annotations for 541 drone orthoimages worldwide. However, the dataset is restricted to 10 cm spatial resolution and contains relatively weak annotations in dense canopies, limiting the ability of models to learn fine canopy structures such as narrow canopy gaps in closed forests [38, 22, 21]. More

generally, current tree cover datasets do not provide coherent joint labels for both tree cover and mortality, which are required for consistent forest vitality assessment [23].

Previous works on tree mortality Recent work has also successfully demonstrated the detection of tree mortality and crown decline (often referred to as standing deadwood) in aerial imagery; in this work, we use the term “mortality” to encompass both. For example, [3] introduced a labeled drone image dataset at 3 cm spatial resolution covering approximately 1,500 ha of *Pinus pinea* forest across nine sites in Pinar de Almorox, Spain. [31] provide 51 labeled orthomosaics from mixed temperate forests in Germany at 1–4 cm resolution. These datasets demonstrate the value of centimeter-scale imagery for detecting fine-grained mortality patterns, but are limited in geographic and ecological scope.

More recently, larger-scale initiatives have emerged. TreeFinder [39] aggregates tree-mortality data at 60 cm spatial resolution from more than 1,000 sites, but is limited to the contiguous United States. In addition, 60 cm resolution is too coarse to reliably detect deciduous dead trees, partial dieback, and other fine-scale mortality signals [9, 22, 32, 16]. Thus, although these datasets are valuable contributions, they remain limited for large-scale forest monitoring in their combined coverage of geographic regions, disturbance types, and fine-scale mortality expression.

The most geographically comprehensive mortality-focused dataset to date was collected through the deadtrees.earth platform (<https://deadtrees.earth>), an initiative designed to crowdsource high-resolution aerial imagery for tree-mortality mapping [20]. The resulting open dataset contains fine-resolution drone imagery (0.01–28 cm) from 434 sites worldwide and enabled training of a globally transferable mortality model [20]. However, it lacks integrated labels for jointly modeling living tree cover and mortality, preventing coherent estimation of relative mortality fraction within forested areas, and it is largely biased toward temperate forests.

Overall, existing datasets reflect a trade-off between spatial resolution, annotation quality, geographic coverage, and label completeness. There is still no globally distributed, centimeter-scale, multi-resolution dataset with coherent annotations for both tree cover and mortality.

3 Datasets: DTE-aerial-train and DTE-aerial-bench

To facilitate large-scale forest monitoring, we curate DTE-aerial-train and DTE-aerial-bench, which are the first globally distributed training and benchmark datasets of centimeter-scale aerial imagery with joint annotations of tree cover and mortality (Table 1). These datasets are constructed from the deadtrees.earth platform [22], where imagery is crowd-sourced globally through collaborations with researchers, ecologists, and environmental monitoring initiatives. Each orthophoto is audited by the deadtrees.earth team and accompanied by detailed metadata, including geocoordinates, biome, acquisition date, contributors, spatial resolution, and licensing information [22]. Our dataset comprises permissively licensed imagery with spatial resolution finer than ≈ 20 cm, acquired between 2012 and 2025, and restricted to the growing season to enable robust discrimination between seasonal leaf senescence and tree mortality.

Multi-resolution To enable generalization across sensors and scales, we construct both the training and test datasets as multi-resolution datasets. The native data is strongly imbalanced toward high-resolution drone imagery (Fig. 1). Following [20], this allows us to generate patches at multiple resolutions via iterative downsampling, producing patches at all target resolutions (2.5, 5, 10, 20 cm) coarser than or equal to the native resolution. This enables coverage from fine to coarse scales while preserving spatial extent (see Appendix for details).

For the benchmark dataset, we restrict orthophotos to resolutions finer than 5 cm, ensuring that each orthophoto can generate corresponding patches at 5, 10, and 20 cm. This design enables consistent cross-scale evaluation of the same underlying scene, minimizing confounding effects from varying native resolutions and ensuring that performance differences can be attributed to scale. In the training set, all orthophotos are tiled into 1024×1024 patches with a 512-pixel overlap, following [20]. We cap the number of patches per orthophoto at 1600 to mitigate bias for overly large orthophotos. In the benchmark set, we instead use non-overlapping 1024×1024 patches.

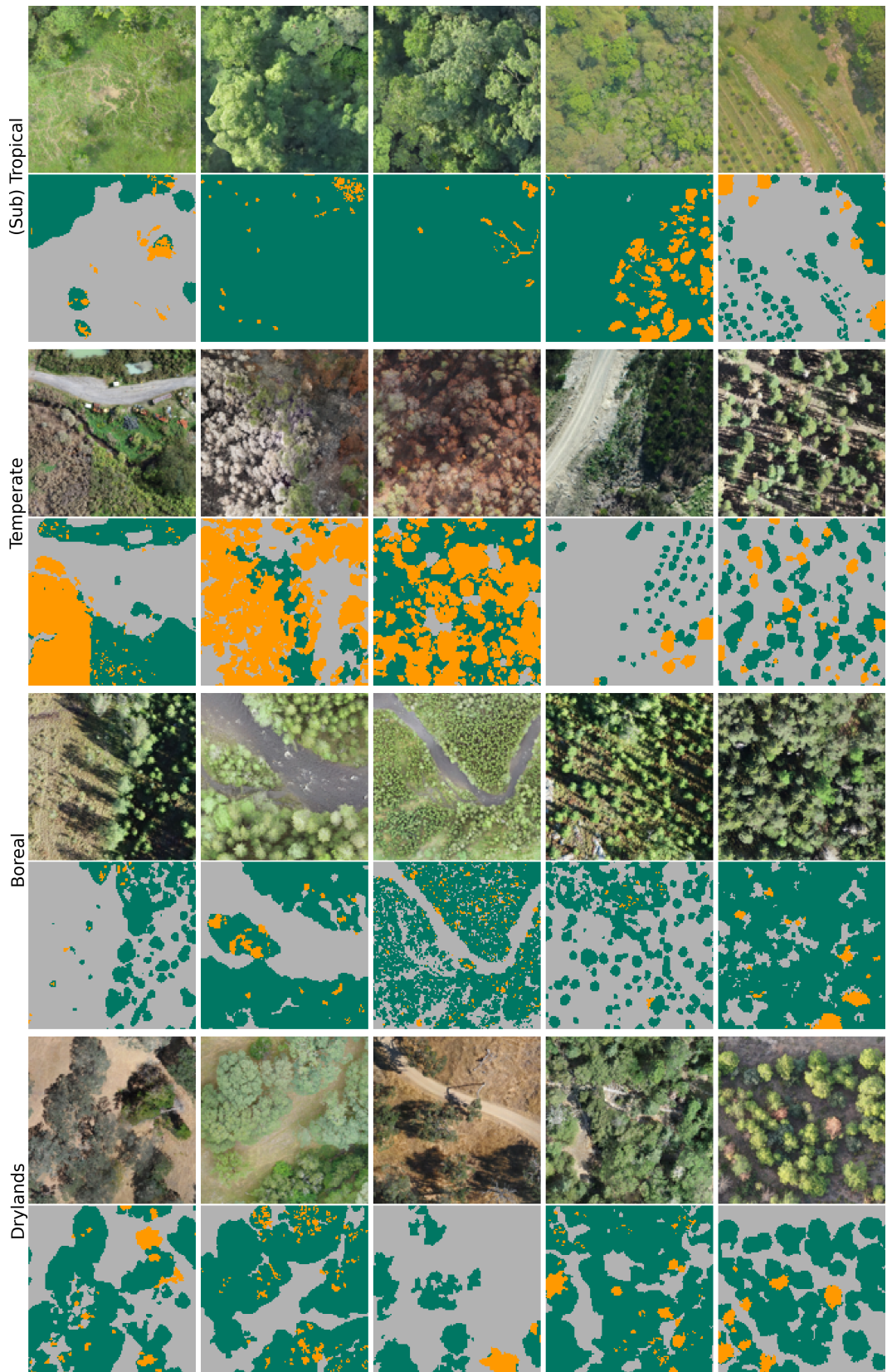


Figure 2: Qualitative examples of aerial imagery tiles and corresponding semantic masks (tree cover: teal, mortality: orange, background: gray) across aggregated biome groups, illustrating diverse canopy structures across ecosystems. We visualize the complete benchmark dataset on deadtrees.earth/releases/dte-aerial-bench.

Spatial and ecological coverage DTE-aerial-train comprises 2,176 globally distributed aerial images, corresponding to 385K image patches (Fig. 1). To reveal ecological coverage, we assign each orthophoto to established global biome definitions based on the coordinates of its centroid [24]. For analysis, biomes are aggregated into four broad groups: temperate, (sub)tropical, drylands (including Mediterranean), and boreal and montane, following [22]. The training dataset is dominated by temperate regions with 1,206 orthophotos (~178K patches), followed by (sub)tropical regions (722 orthophotos, ~149K patches), drylands (194 orthophotos, ~5K patches) and boreal and montane regions (54 orthophotos, ~40K patches).

DTE-aerial-bench comprises 25 orthophotos (525 patches) covering facets of forest structure (e.g. managed and unmanaged forests), biome groups (including 11 temperate, 4 (sub)tropical, 6 dryland, and 4 boreal and montane sites), and mortality stages, where 4 sites include brown- and red-stage mortality, representing recent mortality that is more challenging to detect. Overall, the dataset captures global ecological variability across species composition, forest structure, and environmental gradients Fig. 2.

Annotation pipeline We define three semantic annotation classes: (1) tree cover, (2) mortality, and (3) background. The tree cover class includes standing tree canopies of any size and condition. The mortality class captures a continuum of canopy decline in standing trees from partial dieback to fully dead tree crowns. Background includes scene components such as canopy gaps, bare ground, understory, and other non-tree areas. All classes are annotated via polygons, which enables precise delineation of these classes while remaining more scalable than dense pixel-wise labeling.

The annotation effort required for this task is substantial. Incorporating partial crown dieback into the mortality class is essential for capturing early-stage tree mortality [23, 20], but significantly increases complexity, as partially affected crowns require fine-grained, fragmented, and irregular polygons compared to fully dead trees (Fig. 2). Accurately delineating background regions further adds to this challenge. In particular, canopy gaps, defined as openings in the forest canopy and critical indicators of forest vitality and degradation [13, 26], require precise boundary annotation. Together, these factors make the labeling process considerably more demanding than conventional binary annotation.

To balance annotation quality with scalability, we adopt a two-stage annotation strategy. For the benchmark test set, we prioritize high annotation quality by curating an ecologically representative set of aerial images that are exhaustively labeled across all classes. These images are repeatedly annotated by multiple domain experts, with disagreements resolved through iterative consensus-building to ensure high precision and consistency. All annotations are performed at the highest available resolution (5 cm), and labels at coarser resolutions (e.g., 10 cm, 20 cm) are systematically derived from these base annotations, ensuring consistent cross-scale evaluation (see Appendix Figure 4).

For the training data, we rely on coarsely annotated imagery to achieve extensive geographic coverage while maintaining tractable annotation costs. Labels are initialized for a common set of orthophotos using manually audited pseudo-labels derived with segmentation models of [20] for mortality and [38] for tree cover. As [38] does not reliably capture canopy gaps, we reassign pixels initially labeled as tree cover to background where the vegetation signal is low using heuristic thresholds.

These initial pseudo-labels are iteratively improved through a model-assisted relabeling process. At each stage, models are trained on the current labels and applied to the dataset, after which predictions are reviewed by multiple auditors. Systematic errors identified during this review are used to update the pseudo-labels before retraining the next model iteration. Repeating this process progressively improves label quality while maintaining scalability across the dataset. Additionally, to better capture underrepresented and visually distinct mortality stages, we include a set of eight expert-annotated sites covering brown- and red-stage mortality [22, 20].

In total, 4 annotators and 4 domain experts contributed to dataset curation. Annotators were trained by the domain experts to ensure consistent interpretation of tree mortality signals. Domain experts were closely involved throughout the process, including quality control, disagreement resolution, and iterative feedback. The overall labeling effort amounted to approximately 550 paid person-hours.

Data licensing and usage To enable broad reuse and support open research, we design our dataset around permissive licensing principles. The dataset comprises openly licensed imagery, with most samples released under permissive licenses such as Creative Commons Attribution 4.0 (CC BY 4.0) and the MIT License. Specifically, among the 2,176 aerial images in the DTE-aerial-train,

2,162 are licensed under CC BY 4.0, 9 under the MIT License, and 5 under Creative Commons Attribution–NonCommercial–ShareAlike (CC BY-NC-SA). We distribute all image tiles under the same license as their corresponding source imagery.

Intended use The dataset is designed for developing and *rigorously evaluating* machine learning models for large-scale segmentation of tree cover and tree mortality. The expert-annotated benchmark test set enables standardized comparison across methods, while the larger, coarsely labeled training set reflects realistic constraints such as label noise, class imbalance, and incomplete annotations. Together, they provide a reproducible benchmark for assessing model robustness and generalization across geographic regions, spatial resolutions, and disturbance regimes.

ML problem and ML-ready dataset Our datasets introduce several core challenges for the computer vision community, including (i) long-tailed spatial distributions, (ii) multi-resolution variability across image acquisition scales, (iii) noisy supervision from coarsely labeled data, and (iv) rare out-of-distribution disturbance scenarios. These properties are primarily captured in DTE-aerial-train, which reflects real-world data variability, while DTE-aerial-bench serves as a carefully curated testbed with high-quality, balanced, expert annotations. Together, they define a realistic and controlled benchmark for studying robustness, generalization, and uncertainty-aware learning. In addition, the dataset enables new research directions such as cross-biome generalization under limited training data, transfer across spatial resolutions, and zero-shot adaptation of foundation models to high-resolution aerial imagery.

4 Experiments

Dataset pre-processing and augmentation We randomly split orthophotos of DTE-aerial-train into 90% training and 10% validation, resulting in 1,959 orthophotos (346K patches) for training and 217 orthophotos (39K patches) for validation. All models are trained on random crops of size 640×640 pixels (ablations in Appendix B.4). For regularization, we apply a series of data augmentations, including horizontal and vertical flips, 90-degree rotations, grayscale conversion, gamma adjustments, and color jittering. Finally, input images are normalized using ImageNet statistics.

Backbones and architectures We evaluate a diverse set of segmentation architectures spanning convolutional, transformer-based, and foundation model approaches. For convolutional baselines, we adopt U-Net [29] and DeepLabV3+ (DLV3+) [7] with ResNet-34 and ResNet-50 encoders, implemented using the Segmentation Models PyTorch library [15]. These models are initialized with ImageNet pre-trained weights, which improves convergence over training from scratch. For transformer-based models, we include SegFormer [41] with MiT-B1, and MiT-B3 variants, capturing a range of model capacities. We further evaluate Mask2Former (M2F) [8] in its tiny and small configurations to assess performance under mask-based decoding frameworks. These models are initialized from weights pre-trained on ADE-20K.

Finally, we incorporate foundation model features using the DINOv2 base model with two adaptation strategies [25]. In the single-layer setting (DINOv2^{sl}), only the final transformer layer is used for decoding. In the multi-layer setting (DINOv2^{ml}), intermediate representations from layers 3, 6, 9, 12 are aggregated to capture hierarchical features across the network. Each feature map is projected to 128 channels, concatenated, and passed to a lightweight decoder, enabling the combination of fine-grained spatial details with high-level semantic context in a computationally efficient manner.

Training We use a Tversky loss [1] to address class imbalance. For the background and tree cover classes, we set equal weighting between precision and recall ($\alpha = 0.5$, $\beta = 0.5$). For the mortality class, which is rare and exhibits a long-tailed distribution, we emphasize recall by setting $\alpha = 0.3$ and $\beta = 0.7$, encouraging the model to better capture minority class instances.

Evaluation Our evaluation framework is designed to reflect real-world deployment conditions by assessing model performance across (i) biome groups, (ii) resolution, and (iii) segmentation tasks. We report all results using the F1 score, computed independently for each site and then averaged across sites. Results are reported as the mean and standard deviation over three independent runs with different random seeds (0, 100, 200) to account for variability due to stochastic training dynamics

and random initialization. For each metric, we aggregate performance across runs and present results in the form $\mu \pm 2\sigma$.

Environment impact Models were trained on a single NVIDIA H200 GPU, with the largest model using up to 120 GB VRAM at a 600 W power target and requiring approximately 25 hours of training. Using the Machine Learning Impact calculator [18], we estimate a total carbon footprint of ~ 140 kg CO₂ for all experiments and ablations, excluding testing and failed runs; this estimate likely underestimates total emissions.

Table 2: Comparison of models on mortality and tree cover segmentation performance on the benchmark dataset. We report aggregated F1 for biome groups and resolutions. Results are averaged over 3 seeds, with twice the standard deviation ($\pm 2\sigma$) shown in parentheses. Best results are highlighted in **bold** and second-best in *italics*.

Model	Temperate	Tropical	Boreal	Drylands	5cm	10cm	20cm
Mortality (F1)							
DT-V1 [20]	0.51	0.64	0.40	0.55	0.55	0.47	0.39
MiT-B3	0.58 (± 0.04)	<i>0.66</i> (± 0.00)	0.58 (± 0.01)	0.56 (± 0.04)	0.60 (± 0.03)	0.55 (± 0.02)	0.45 (± 0.01)
MiT-B1	<i>0.56</i> (± 0.02)	0.67 (± 0.01)	<i>0.57</i> (± 0.02)	<i>0.57</i> (± 0.00)	0.60 (± 0.00)	<i>0.54</i> (± 0.02)	0.43 (± 0.01)
U-Net(res34)	0.53 (± 0.01)	0.65 (± 0.01)	0.53 (± 0.02)	0.59 (± 0.01)	<i>0.58</i> (± 0.00)	0.52 (± 0.01)	0.40 (± 0.02)
U-Net(res50)	0.52 (± 0.02)	<i>0.64</i> (± 0.01)	0.51 (± 0.00)	0.59 (± 0.01)	<i>0.57</i> (± 0.01)	0.52 (± 0.01)	0.42 (± 0.02)
M2F(s)	0.53 (± 0.04)	0.67 (± 0.00)	<i>0.57</i> (± 0.01)	<i>0.58</i> (± 0.02)	<i>0.58</i> (± 0.02)	<i>0.54</i> (± 0.01)	0.43 (± 0.01)
M2F(t)	0.53 (± 0.02)	0.67 (± 0.01)	<i>0.57</i> (± 0.01)	0.55 (± 0.02)	<i>0.58</i> (± 0.01)	<i>0.54</i> (± 0.01)	<i>0.44</i> (± 0.01)
DLV3+(res34)	0.53 (± 0.02)	0.65 (± 0.01)	0.52 (± 0.00)	0.56 (± 0.00)	<i>0.58</i> (± 0.01)	0.50 (± 0.02)	0.38 (± 0.04)
DLV3+(res50)	0.51 (± 0.01)	0.65 (± 0.00)	0.54 (± 0.01)	0.56 (± 0.01)	<i>0.57</i> (± 0.01)	0.49 (± 0.01)	0.39 (± 0.03)
DINOv2(b) ^{ml}	0.41 (± 0.01)	0.63 (± 0.01)	0.42 (± 0.01)	0.54 (± 0.01)	0.49 (± 0.00)	0.46 (± 0.00)	0.37 (± 0.01)
DINOv2(b) ^{sl}	0.39 (± 0.02)	0.63 (± 0.00)	0.40 (± 0.00)	0.53 (± 0.01)	0.47 (± 0.00)	0.44 (± 0.01)	0.36 (± 0.01)
Tree cover (F1)							
TCD [38]	0.89	<i>0.91</i>	0.91	0.91	0.90	0.91	0.87
MiT-B3	0.85 (± 0.01)	0.92 (± 0.00)	0.93 (± 0.00)	0.93 (± 0.00)	0.89 (± 0.00)	0.89 (± 0.00)	0.89 (± 0.00)
MiT-B1	0.85 (± 0.00)	<i>0.91</i> (± 0.00)	0.93 (± 0.00)	<i>0.92</i> (± 0.00)	0.89 (± 0.00)	0.89 (± 0.00)	0.89 (± 0.00)
U-Net(res50)	0.84 (± 0.00)	0.92 (± 0.00)	<i>0.92</i> (± 0.00)	<i>0.92</i> (± 0.00)	0.88 (± 0.00)	<i>0.90</i> (± 0.00)	<i>0.88</i> (± 0.00)
U-Net(res34)	<i>0.85</i> (± 0.01)	0.92 (± 0.01)	<i>0.92</i> (± 0.00)	<i>0.92</i> (± 0.00)	<i>0.89</i> (± 0.01)	<i>0.90</i> (± 0.00)	<i>0.88</i> (± 0.00)
M2F(s)	0.85 (± 0.02)	0.92 (± 0.01)	0.93 (± 0.00)	<i>0.92</i> (± 0.00)	0.89 (± 0.00)	<i>0.90</i> (± 0.01)	0.89 (± 0.00)
M2F(t)	0.84 (± 0.01)	0.92 (± 0.01)	0.93 (± 0.00)	<i>0.92</i> (± 0.00)	0.89 (± 0.00)	0.89 (± 0.01)	0.89 (± 0.01)
DLV3+(res50)	0.84 (± 0.01)	<i>0.91</i> (± 0.00)	0.93 (± 0.00)	<i>0.92</i> (± 0.00)	0.89 (± 0.00)	0.89 (± 0.01)	<i>0.88</i> (± 0.00)
DLV3+(res34)	0.84 (± 0.00)	<i>0.91</i> (± 0.01)	<i>0.92</i> (± 0.00)	<i>0.92</i> (± 0.00)	0.89 (± 0.00)	0.89 (± 0.01)	<i>0.88</i> (± 0.00)
DINOv2(b) ^{ml}	0.84 (± 0.00)	<i>0.91</i> (± 0.01)	0.87 (± 0.01)	0.89 (± 0.00)	0.87 (± 0.01)	0.87 (± 0.00)	0.84 (± 0.00)
DINOv2(b) ^{sl}	0.84 (± 0.00)	<i>0.91</i> (± 0.00)	0.87 (± 0.00)	0.88 (± 0.00)	0.87 (± 0.00)	0.86 (± 0.00)	0.84 (± 0.00)

5 Results and Discussion

In Table 2, we evaluate baseline models on DTE-aerial-bench across biomes and spatial resolutions to assess generalization under ecological and sensor variability. For mortality, compared to the DT-V1 [20], most models consistently improve segmentation performance across biomes when trained on DTE-aerial-train. The strongest gains are observed in the boreal and montane biome group, with MiT-B3 achieving a +45% relative improvement in boreal forests (0.40 \rightarrow 0.58). Additional improvements are observed in temperate forests (+13.7%, 0.51 \rightarrow 0.58), while gains in tropical forests (+3.1%) and drylands (+1.8%) are modest, remaining close to the baseline. The boreal biome remains the most challenging due to data sparsity, while the large relative improvement highlights the robustness of the learned representations. Performance in dryland forests remains competitive with the baseline. Performance improvements are further consistent across spatial resolutions. Compared to DT-V1, MiT-B3 achieves a +9.1% relative improvement at 5 cm (0.55 \rightarrow 0.60), +17.0% at 10 cm (0.47 \rightarrow 0.55), and +15.4% at 20 cm (0.39 \rightarrow 0.45). This trend suggests that our approach is particularly effective at leveraging contextual information when fine-grained spatial details are degraded.

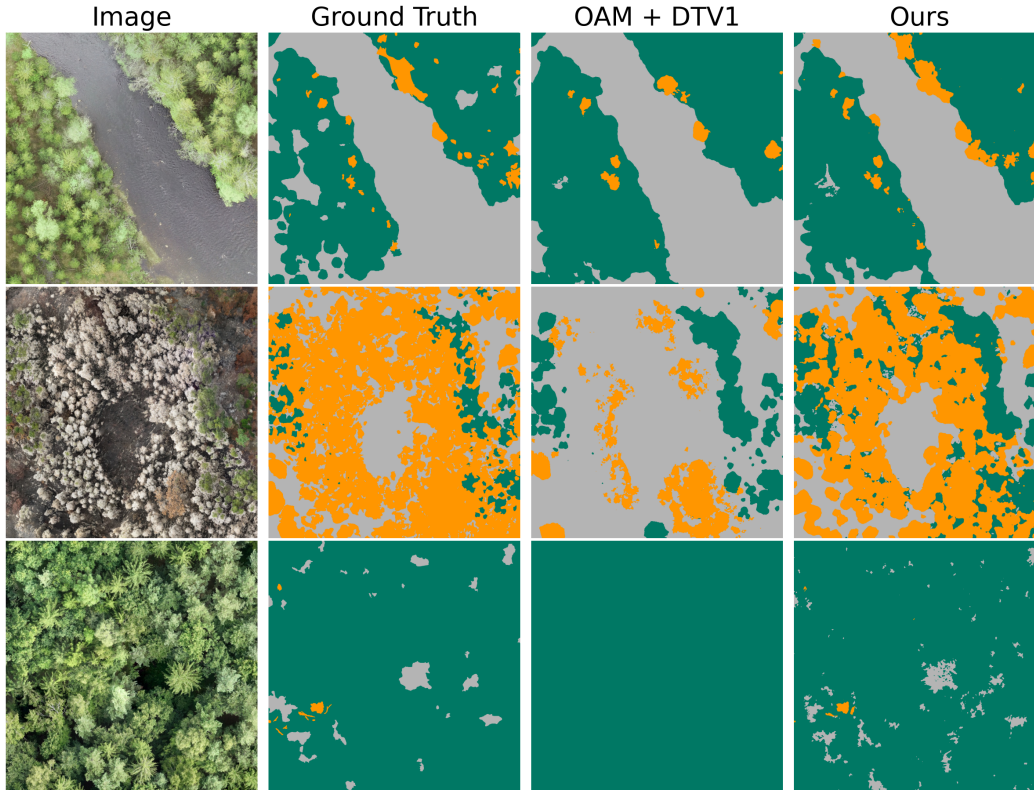


Figure 3: Qualitative comparison of segmentations on benchmark patches. Our method produces more consistent delineation of tree cover and mortality than combined baselines from OAM and DTV1 [38, 20]. Predictions for $> 7K$ orthoimages can be inspected on [deadtrees.earth/dataset](https://deadtrees.eearth.org/dataset).

In addition to improved mortality detection, the joint setting enables consistent estimation of tree cover, allowing relative mortality to be quantified within forested areas. Compared to the OAM baseline [38], which operates near saturation, performance remains on par across most biomes and spatial resolutions, indicating that joint learning preserves strong tree cover performance, with a moderate decrease in temperate forests ($0.89 \rightarrow 0.85$).

Overall, MiT-B3 provides the best balance across both tasks, delivering substantial improvements for mortality (+11.3%) while maintaining competitive performance for tree cover relative to a strong baseline (Appendix Table 3). These results highlight the ability of the proposed dataset and models to jointly capture rare, spatially heterogeneous patterns alongside dominant large-scale structures.

6 Conclusion

We introduced *DTE-aerial-train* and *DTE-aerial-bench*, a global, multi-resolution aerial image resource for joint segmentation of tree cover and mortality. By combining large-scale, coarsely annotated training data with an expert-annotated benchmark test set, the dataset enables standardized evaluation under realistic variation in biome, spatial resolution, and mortality expression. Our baselines demonstrate that joint training improves mortality detection, particularly in challenging forests and mortality scenarios, while maintaining strong tree-cover performance. We hope this resource supports reproducible progress in robust forest monitoring and serves as a challenging benchmark for advancing generalization, uncertainty-aware learning, and segmentation under real-world distribution shifts.

Ethics, Limitations and Impact We expect that the release of this dataset will support progress in large-scale ecological monitoring and tree mortality assessment. However, several limitations should be considered. First, the dataset is derived from aerial imagery without systematic validation against

in-situ field measurements; therefore, models trained on this data should not be used for operational or decision-making purposes without additional local validation. Second, despite careful curation and multi-stage quality control, the annotations contain inherent uncertainty due to human interpretation, especially in visually ambiguous cases such as partial canopy mortality or shadow effects. Third, the dataset is not uniformly distributed across biomes and geographic regions. While we aim for broad ecological coverage, some environments (e.g., boreal and drylands) remain limited, which may affect generalization. Finally, the dataset is biased toward high-resolution imagery (<20–30 cm), making models less directly transferable to lower-resolution airplane or satellite data without adaptation.

Acknowledgments and Disclosure of Funding

C.M. and T.K. thank the European Space Agency for funding the “DeepFeatures” project via the AI4SCIENCE activity and the “FORTRACK” project via the ESA CLIMATE SPACE: Climate–Biodiversity studies. C.M. acknowledges financial support from the German Aerospace Centre (DLR) on behalf of the Federal Ministry for Economic Affairs and Climate Action (BMWK) for project ML4Earth (FKZ 50EE2201B).

References

- [1] Abraham, N., Khan, N.M.: A novel focal tversky loss function with improved attention u-net for lesion segmentation. In: 2019 IEEE 16th international symposium on biomedical imaging (ISBI 2019). pp. 683–687. IEEE (2019)
- [2] Allen, C.D., Breshears, D.D., McDowell, N.G.: On underestimation of global vulnerability to tree mortality and forest die-off from hotter drought in the anthropocene. *Ecosphere* **6**(8), 1–55 (2015)
- [3] Allen, M.J., Moreno-Fernández, D., Ruiz-Benito, P., Grieve, S.W., Lines, E.R.: Low-cost tree crown dieback estimation using deep learning-based segmentation. *Environmental Data Science* **3**, e18 (2024)
- [4] Allen, M.J., Owen, H.J., Grieve, S.W., Lines, E.R.: Manual labelling artificially inflates deep learning-based segmentation performance on rgb images of closed canopy: validation using tls. arXiv preprint arXiv:2503.14273 (2025)
- [5] Bachelet, D., Neilson, R.P., Hickler, T., Drapek, R.J., Lenihan, J.M., Sykes, M.T., Smith, B., Sitch, S., Thonicke, K.: Simulating past and future dynamics of natural ecosystems in the united states. *Global Biogeochemical Cycles* **17**(2) (2003)
- [6] Ball, J.G., Hickman, S.H., Jackson, T.D., Koay, X.J., Hirst, J., Jay, W., Archer, M., Aubry-Kientz, M., Vincent, G., Coomes, D.A.: Accurate delineation of individual tree crowns in tropical forests from aerial rgb imagery using mask r-cnn. *Remote Sensing in Ecology and Conservation* **9**(5), 641–655 (2023)
- [7] Chen, L.C., Zhu, Y., Papandreou, G., Schroff, F., Adam, H.: Encoder-decoder with atrous separable convolution for semantic image segmentation. In: Proceedings of the European conference on computer vision (ECCV). pp. 801–818 (2018)
- [8] Cheng, B., Misra, I., Schwing, A.G., Kirillov, A., Girdhar, R.: Masked-attention mask transformer for universal image segmentation. In: Proceedings of the IEEE/CVF conference on computer vision and pattern recognition. pp. 1290–1299 (2022)
- [9] Cheng, Y., Oehmcke, S., Brandt, M., Rosenthal, L., Das, A., Vrieling, A., Saatchi, S., Wagner, F., Mugabowindekwe, M., Verbruggen, W., et al.: Scattered tree death contributes to substantial forest loss in california. *Nature communications* **15**(1), 641 (2024)
- [10] Cloutier, M., Germain, M., Laliberté, E.: Influence of temperate forest autumn leaf phenology on segmentation of tree species from uav imagery using deep learning. *Remote Sensing of Environment* **311**, 114283 (2024)

- [11] Duguay, S.O., Baudchon, H., Laliberté, E., Muller-Landau, H., Rivas-Torres, G., Ouaknine, A.: Selvamask: Segmenting trees in tropical forests and beyond. arXiv preprint arXiv:2602.02426 (2026)
- [12] Friedlingstein, P., O’sullivan, M., Jones, M.W., Andrew, R.M., Bakker, D.C., Hauck, J., Landschützer, P., Le Quéré, C., Luijkx, I.T., Peters, G.P., et al.: Global carbon budget 2023. *Earth System Science Data* **15**(12), 5301–5369 (2023)
- [13] Hagemann, N., Magdon, P., Schnell, S., Pommerening, A.: Analysing gap dynamics in forest canopies with landscape metrics based on multi-temporal airborne laser scanning surveys—a pilot study. *Ecological Indicators* **145**, 109627 (2022)
- [14] Hartmann, H., Bastos, A., Das, A.J., Esquivel-Muelbert, A., Hammond, W.M., Martínez-Vilalta, J., McDowell, N.G., Powers, J.S., Pugh, T.A., Ruthrof, K.X., et al.: Climate change risks to global forest health: emergence of unexpected events of elevated tree mortality worldwide. *Annual review of plant biology* **73**(1), 673–702 (2022)
- [15] Iakubovskii, P.: Segmentation models pytorch. github. GitHub repository https://github.com/qubvel/segmentation_models_pytorch (2019)
- [16] Kattenborn, T., Leitloff, J., Schiefer, F., Hinz, S.: Review on convolutional neural networks (cnn) in vegetation remote sensing. *ISPRS journal of photogrammetry and remote sensing* **173**, 24–49 (2021)
- [17] Khatri-Chhetri, P., van Wagtenonk, L., Hendryx, S.M., Kane, V.R.: Enhancing individual tree mortality mapping: The impact of models, data modalities, and classification taxonomy. *Remote Sensing of Environment* **300**, 113914 (2024)
- [18] Lacoste, A., Luccioni, A., Schmidt, V., Dandres, T.: Quantifying the carbon emissions of machine learning. arXiv preprint arXiv:1910.09700 (2019)
- [19] Migliavacca, M., Grassi, G., Bastos, A., Ceccherini, G., Ciais, P., Janssens-Maenhout, G., Lugato, E., Mahecha, M.D., Novick, K.A., Peñuelas, J., et al.: Securing the forest carbon sink for the european union’s climate ambition. *Nature* **643**(8074), 1203–1213 (2025)
- [20] Möhring, J., Kattenborn, T., Mahecha, M.D., Cheng, Y., Schwenke, M.B., Cloutier, M., Denter, M., Frey, J., Gassilloud, M., Göritz, A., et al.: Global, multi-scale standing deadwood segmentation in centimeter-scale aerial images. *Authorea Preprints* (2025)
- [21] Mosig, C., Kattenborn, T., Loaiza, D.M., Vanja-Jehle, J., Brandt, J., Jacobs, N., Khanal, S., Xing, E., Schwartz, M., Muller-Landau, H.C., et al.: Sub-pixel mapping of disturbance and tree mortality dynamics from sentinel-2 time series around the globe (2026)
- [22] Mosig, C., Vajna-Jehle, J., Mahecha, M.D., Cheng, Y., Hartmann, H., Montero, D., Junttila, S., Horion, S., Schwenke, M.B., Koontz, M.J., Maulud, K.N.A., Adu-Bredu, S., Al-Halbouni, D., Ali, M., Allen, M., Altman, J., Amorós, L., Angiolini, C., Astrup, R., Awada, H., Barrasso, C., Bartholomeus, H., Beck, P.S., Bozzini, A., Braun-Wimmer, J., Brede, B., Breunig, F.M., Brugnaro, S., Buras, A., Burchard-Levine, V., Camarero, J.J., Candotti, A., Capuder, L., Carrieri, E., Centritto, M., Chirici, G., Cloutier, M., Conciani, D., Cushman, K., Dalling, J.W., Dao, P.D., Dempewolf, J., Denter, M., Dogotari, M., Díaz-Delgado, R., Ecke, S., Eichel, J., Eltner, A., Fabbri, A., Fabi, M., Fassnacht, F., Ferreira, M.P., Fischer, F.J., Frey, J., Frick, A., Fuentes, J., Ganz, S., Garbarino, M., García, M., Gassilloud, M., Gazol, A., Gea-Izquierdo, G., Gerberding, K., Ghasemi, M., Giannetti, F., Gillan, J., Gonzalez, R., Gosper, C., Greene, T., Greinwald, K., Grieve, S., Große-Stoltenberg, A., Gutierrez, J.A., Göritz, A., Hajek, P., Hedding, D., Hempel, J., Heremans, S., Hernández, M., Heurich, M., Honkavaara, E., Höfle, B., Jackisch, R., Jucker, T., Kalwij, J.M., Kepfer-Rojas, S., Khatri-Chhetri, P., Kleinebecker, T., Klemmt, H.J., Klouček, T., Koivumäki, N., Kolagani, N., Komárek, J., Korznikov, K., Kraszewski, B., Kruse, S., Krüger, R., Kuechly, H., Kwong, I.H., Laliberté, E., Langan, L., Latifi, H., Leal-Medina, C., Lehmann, J.R., Li, L., Lines, E., Lisiewicz, M., Lopatin, J., Lucieer, A., Ludwig, A., Ludwig, M., Lyytikäinen-Saarenmaa, P., Ma, Q., Mansuy, N., Peña, J.M., Marino, G., Maroschek, M., Martín, M., Martín-Benito, D., Matham, P., Mazzoni, S., Meloni, F., Menzel, A., Meyer, H., Miraki, M., Moreno, G., Moreno-Fernández, D., Muller-Landau, H.C., Mälicke, M., Möhring,

- J., Müllerova, J., Naidu, S.S., Nardi, D., Neumeier, P., Nita, M.D., Näsi, R., Oppgenorth, L., Orunbaev, S., Palmer, M., Paul, T., Pfenning, M., Potts, A., Prasanna, G.L., Prober, S., Puliti, S., Pérez-Luque, A.J., Pérez-Priego, O., Reudenbach, C., Revuelto, J., Rivas-Torres, G., Roberge, P., Roggero, P.P., Rossi, C., Ruehr, N.K., Ruiz-Benito, P., Runge, C.M., Satta, G.G.A., Scanu, B., Scherer-Lorenzen, M., Schiefer, F., Schiller, C., Schladebach, J., Schmehl, M.T., Schmid, J., Schmidt, T.A., Schwarz, S., Seidl, R., Seifert, T., Barba, A.S., Shafeian, E., Shapiro, A., de Simone, L., Sohrabi, H., Soltani, S., Sotomayor, L., Sparrow, B., Steer, B.S., Stenson, M., Stöckigt, B., Su, Y., Suomalainen, J., Tamudo, E., Barbieri, M.J.T., Tomelleri, E., Torresani, M., Trepekli, K., Ullah, S., Ullah, S., Umlauf, J., Vargas-Ramírez, N., Vatandaslar, C., Visacki, V., Volpi, M., Vásquez, V., Wallis, C., Weinstein, B., Weiser, H., Wich, S., Ximena, T.C., Zarco-Tejada, P.J., Zdunic, K., Zielewska-Büttner, K., de Oliveira, R.A., van Wagendonk, L., von Dösky, V., Kattenborn, T.: deadtrees.earth - an open-access and interactive database for centimeter-scale aerial imagery to uncover global tree mortality dynamics. *Remote Sensing of Environment* **332**, 115027 (2026). <https://doi.org/https://doi.org/10.1016/j.rse.2025.115027>, <https://www.sciencedirect.com/science/article/pii/S0034425725004316>
- [23] Network, I.T.M., Senf, C., Esquivel-Muelbert, A., Pugh, T.A., Anderegg, W.R., Anderson-Teixeira, K.J., Arellano, G., Beloiu Schwenke, M., Bentz, B.J., Boehmer, H.J., et al.: Towards a global understanding of tree mortality. *New Phytologist* **245**(6), 2377–2392 (2025)
- [24] Olson, D.M., Dinerstein, E., Wikramanayake, E.D., Burgess, N.D., Powell, G.V., Underwood, E.C., D’Amico, J.A., Itoua, I., Strand, H.E., Morrison, J.C., et al.: Terrestrial ecoregions of the world: A new map of life on earth: A new global map of terrestrial ecoregions provides an innovative tool for conserving biodiversity. *BioScience* **51**(11), 933–938 (2001)
- [25] Oquab, M., Darcet, T., Moutakanni, T., Vo, H., Szafraniec, M., Khalidov, V., Fernandez, P., Haziza, D., Massa, F., El-Nouby, A., et al.: Dinov2: Learning robust visual features without supervision. *arXiv preprint arXiv:2304.07193* (2023)
- [26] Perry, D.A., Oren, R., Hart, S.C.: *Forest ecosystems*. JHU press (2008)
- [27] Polewski, P., Yao, W., Heurich, M., Krzystek, P., Stilla, U.: Detection of single standing dead trees from aerial color infrared imagery by segmentation with shape and intensity priors. *ISPRS Annals of the Photogrammetry, Remote Sensing and Spatial Information Sciences* **2**, 181–188 (2015)
- [28] Raffa, K.F., Aukema, B.H., Bentz, B.J., Carroll, A.L., Hicke, J.A., Turner, M.G., Romme, W.H.: Cross-scale drivers of natural disturbances prone to anthropogenic amplification: the dynamics of bark beetle eruptions. *Bioscience* **58**(6), 501–517 (2008)
- [29] Ronneberger, O., Fischer, P., Brox, T.: U-net: Convolutional networks for biomedical image segmentation. In: *International Conference on Medical image computing and computer-assisted intervention*. pp. 234–241. Springer (2015)
- [30] Schiefer, F., Frey, J., Kattenborn, T.: Fortress: Forest tree species segmentation in very-high resolution uav-based orthomosaics (2022). <https://doi.org/10.35097/538>, <https://doi.org/10.35097/538>
- [31] Schiefer, F., Kattenborn, T., Frick, A., Frey, J., Schall, P., Koch, B., Schmidlein, S.: Mapping forest tree species in high resolution uav-based rgb-imagery by means of convolutional neural networks. *ISPRS Journal of Photogrammetry and Remote Sensing* **170**, 205–215 (2020)
- [32] Schiefer, F., Schmidlein, S., Frick, A., Frey, J., Klinke, R., Zielewska-Büttner, K., Junntila, S., Uhl, A., Kattenborn, T.: Uav-based reference data for the prediction of fractional cover of standing deadwood from sentinel time series. *ISPRS Open Journal of Photogrammetry and Remote Sensing* **8**, 100034 (2023)
- [33] Schiefer, F., Schmidlein, S., Hartmann, H., Schnabel, F., Kattenborn, T.: Large-scale remote sensing reveals that tree mortality in germany appears to be greater than previously expected. *Forestry: An International Journal of Forest Research* p. cpae062 (2024)
- [34] Scholze, M., Knorr, W., Arnell, N.W., Prentice, I.C.: A climate-change risk analysis for world ecosystems. *Proceedings of the national academy of sciences* **103**(35), 13116–13120 (2006)

- [35] Troles, J., Schmid, U., Fan, W., Tian, J.: Bamforests: Bamberg benchmark forest dataset of individual tree crowns in very-high-resolution uav images. *Remote Sensing* **16**(11), 1935 (2024)
- [36] Trumbore, S., Brando, P., Hartmann, H.: Forest health and global change. *Science* **349**(6250), 814–818 (2015)
- [37] Vasquez, V., Cushman, K., Ramos, P., Williamson, C., Villareal, P., Gomez, C.L., Muller-Landau, H.: Barro colorado island 50-ha plot crown maps: manuallysegmented and instance segmented.(version 2). smithsonian tropical research institute (2023)
- [38] Veitch-Michaelis, J., Cottam, A., Schweizer, D., Broadbent, E., Dao, D., Zhang, C., Almeyda Zambrano, A., Max, S.: Oam-tcd: A globally diverse dataset of high-resolution tree cover maps. *Advances in neural information processing systems* **37**, 49749–49767 (2024)
- [39] Wang, Z., Li, C., Wang, R., Ma, L., Hurtt, G., Jia, X., Mai, G., Li, Z., Xie, Y.: Treefinder: A us-scale benchmark dataset for individual tree mortality monitoring using high-resolution aerial imagery. In: *The Thirty-ninth Annual Conference on Neural Information Processing Systems Datasets and Benchmarks Track*
- [40] Weinstein, B., Marconi, S., White, E.: Training data for the neontreeevaluation benchmark (2020)
- [41] Xie, E., Wang, W., Yu, Z., Anandkumar, A., Alvarez, J.M., Luo, P.: Segformer: Simple and efficient design for semantic segmentation with transformers. *Advances in neural information processing systems* **34**, 12077–12090 (2021)

A Data appendices

A.1 Data preprocessing - DTE-aerial-train

We applied a standardized preprocessing pipeline consisting of polygon label rasterization, reprojection, multi-scale resampling, and tiling to transform heterogeneous raw data from *deadtrees.earth* into a consistent format suitable for model training.

Label rasterization Following [20], vector annotations delineating mortality and tree cover are converted into pixel-wise masks aligned with the original orthophotos. Pixels corresponding to tree cover are assigned a value of 1, mortality pixels a value of 2, while background pixels are assigned 0.

The datasets obtained from *deadtrees.earth* provide careful labels of high- and low-quality image regions, labeled as inside and outside of the Area of Interest (AOI) during the platform’s data audit [22]. Here, regions outside the AOI are marked with a void label (255) and excluded from both loss computation and evaluation. This allows the use of tiles that partially extend beyond annotated regions without introducing training noise. Inclusion of such partial tiles is critical to creating a robust prediction model that can handle the often jagged border of drone orthophotos.

Reprojection. To harmonize spatial representations, we reproject all orthophotos and corresponding masks to their respective Universal Transverse Mercator (UTM) zones, determined from the WGS84 centroid of each image [20]. The resampling was performed using GDAL with cubic convolution resampling and nearest neighbour resampling for imagery and masks, respectively. This transformation places all data in a consistent metric and local coordinate system (meters), ensuring that spatial patterns, object sizes, and distances are represented uniformly across samples. Such consistency is critical for learning robust spatial features, as it prevents scale ambiguities and geometric distortions that could otherwise degrade model training and limit generalization across sites and sensors [32].

Multi-scale resampling The crowd-sourced drone and airplane imagery in *deadtrees.earth* spans multiple spatial resolutions due to varying flight altitudes and sensors. To improve robustness to this variability, we augment the dataset through multi-scale resampling [20]. Each orthophoto is resampled to a fixed set of target spatial resolutions, 2.5 cm, 5 cm, 10 cm, and 20 cm. For instance, an image originally captured at 1.5 cm is downsampled to all coarser resolutions, exposing the model to a broad range of spatial scales during training.

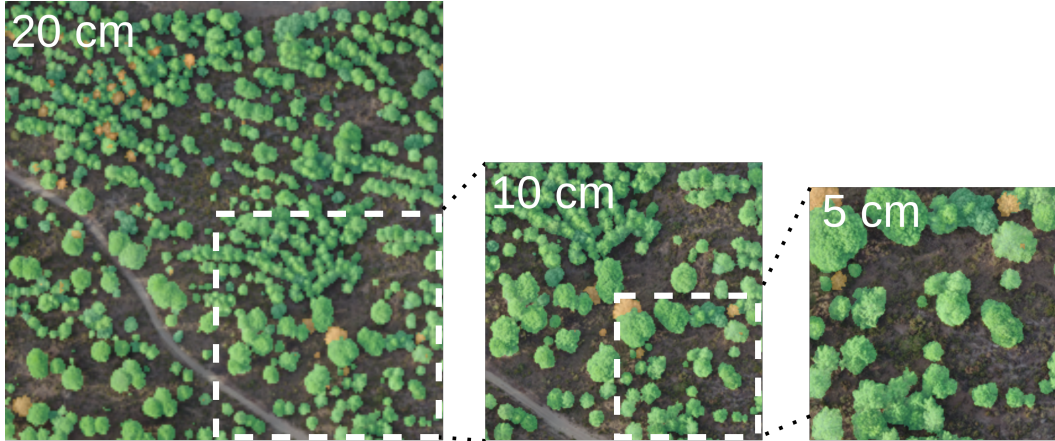


Figure 4: Multi-scale annotation and resampling in DTE-aerial-bench. Labels are created at 5 cm spatial resolution (right) and propagated to 10 cm and 20 cm via downsampling. This ensures consistent annotations across spatial scales. We visualize all patches of the benchmark dataset across resolutions on deadtrees.earth/benchmark-datasets/dte-aerial-bench.

Tiling All images and masks are partitioned into fixed-size tiles of 1024×1024 pixels, extracted with 50% overlap. Tiles containing more than 30% void pixels are discarded. We retain tiles with no mortality instances, as they provide essential negative examples that help the model generalize to non-forest regions and healthy canopy areas. After tiling, we sample at most 1600 tiles per orthophoto to mitigate bias from overly large images. Sampling is balanced across resolutions, with 400 patches drawn from each spatial resolution (2.5 cm, 5 cm, 10 cm, and 20 cm). Within each resolution, we further enforce class balance by selecting 200 patches containing mortality instances (>0 pixels) and 200 without.

A.2 Data preprocessing - DTE-aerial-bench

For DTE-aerial-bench, we developed a web-based annotation tool on the *deadtrees.earth* platform to effectively assist annotators in labeling the large data files, while also enabling collaborative and iterative labeling. In this web-interface, annotators labeled high-resolution aerial imagery at 5 cm spatial resolution using a fixed set of 16 tiles per site. Labels at coarser resolutions (10 cm and 20 cm) were generated automatically through downsampling (see Fig. 4), resulting in 16 tiles at 5 cm, 4 tiles at 10 cm, and 1 tile at 20 cm per site, and a total of 21 tiles per site. The annotation tool also incorporated a quality control workflow with multi-reviewer validation. Only patches approved by multiple reviewers for both mortality and tree cover were retained in the final benchmark.

B Technical appendices and supplementary material

B.1 Hyperparameters and early stopping

We train all models with a batch size of 32 using the AdamW optimizer with weight decay 0.01 and momentum parameters $\beta_1 = 0.9$ and $\beta_2 = 0.99$. A cosine learning rate schedule is used, decaying from 1×10^{-4} to 1×10^{-5} over 100K training iterations.

We use early stopping based on the mean per-site F1-score, computed by averaging F1-scores across sites to reduce bias toward sites with many patches. Training stops if either the mortality F1-score or the mean F1-score across all classes fails to improve by at least 1×10^{-3} over two consecutive evaluation epochs (approximately 21K iterations).

B.2 Class-level model evaluation

We evaluate class-level performance in Table 3 using F1 score, Intersection over Union (IoU), precision, and recall. All models, except the foundational model (DINOv2), outperform the baseline

on mortality detection. In particular, MiT-B3 achieves a substantial improvement for mortality (+11.3% relative improvement), while maintaining performance comparable to strong baselines on tree cover.

Table 3: Class-level evaluation on mortality and tree cover. We report F1, IoU, Precision and Recall for tree cover and mortality.

Model	Mortality				Tree Cover			
	F1	IoU	Prec.	Recall	F1	IoU	Prec.	Recall
DT-V1 [20]	0.53	0.39	0.69	0.47	–	–	–	–
OAM [38]	–	–	–	–	0.90	0.84	0.86	0.96
MiT-B3	0.59 (± 0.02)	0.45 (± 0.02)	0.72 (± 0.02)	0.54 (± 0.04)	0.89 (± 0.00)	0.83 (± 0.00)	0.88 (± 0.01)	0.92 (± 0.01)
MiT-B1	0.58 (± 0.01)	0.44 (± 0.01)	0.71 (± 0.02)	0.53 (± 0.02)	0.89 (± 0.00)	0.82 (± 0.00)	0.87 (± 0.00)	0.93 (± 0.00)
U-Net(res50)	0.55 (± 0.01)	0.42 (± 0.01)	0.70 (± 0.00)	0.51 (± 0.01)	0.88 (± 0.00)	0.81 (± 0.00)	0.87 (± 0.01)	0.92 (± 0.01)
U-Net(res34)	0.56 (± 0.00)	0.42 (± 0.00)	0.70 (± 0.00)	0.52 (± 0.01)	0.89 (± 0.00)	0.82 (± 0.00)	0.87 (± 0.00)	0.92 (± 0.00)
M2F(s)	0.57 (± 0.02)	0.43 (± 0.02)	0.71 (± 0.01)	0.52 (± 0.03)	0.89 (± 0.01)	0.82 (± 0.00)	0.87 (± 0.01)	0.93 (± 0.00)
M2F(t)	0.56 (± 0.00)	0.43 (± 0.00)	0.71 (± 0.02)	0.51 (± 0.01)	0.89 (± 0.00)	0.82 (± 0.01)	0.87 (± 0.01)	0.92 (± 0.00)
DLV3+(res50)	0.55 (± 0.01)	0.41 (± 0.01)	0.71 (± 0.01)	0.49 (± 0.01)	0.88 (± 0.00)	0.82 (± 0.00)	0.87 (± 0.00)	0.92 (± 0.00)
DLV3+(res34)	0.56 (± 0.01)	0.42 (± 0.01)	0.70 (± 0.01)	0.51 (± 0.02)	0.89 (± 0.00)	0.82 (± 0.00)	0.87 (± 0.00)	0.92 (± 0.01)
DINOv2(b) ^{ml}	0.48 (± 0.00)	0.34 (± 0.00)	0.62 (± 0.01)	0.45 (± 0.01)	0.87 (± 0.01)	0.78 (± 0.01)	0.83 (± 0.01)	0.92 (± 0.00)
DINOv2(b) ^{sl}	0.46 (± 0.01)	0.33 (± 0.00)	0.62 (± 0.01)	0.45 (± 0.01)	0.87 (± 0.00)	0.78 (± 0.00)	0.83 (± 0.00)	0.92 (± 0.00)

B.3 Ablation on loss function

In Table 4, we analyze the impact of the loss function. Given the long-tailed and spatially heterogeneous nature of mortality detection, we adopt Tversky loss to bias optimization toward recall ($\alpha = 0.3$, $\beta = 0.7$), improving detection of the rare mortality class while tolerating controlled false positives. We compare this to Dice loss, which equally weights precision and recall (i.e., $\alpha = \beta = 0.5$). Tversky loss improves mortality detection across all spatial scales, with modest gains across most biomes and the largest improvement in temperate regions (+9.4% relative gain, 0.51 \rightarrow 0.56). Overall, this leads to improved mortality performance while maintaining competitive tree cover performance.

B.4 Ablation on image patch size

To assess the impact of patch size, which determines the spatial context available to the model for capturing mortality and tree cover patterns, we perform an ablation over patch sizes of 224, 512, and 640 (Table 4). For mortality, larger patch sizes (640) generally perform slightly better across spatial resolutions, while performance across biomes remains comparable, with no single configuration consistently dominating. This suggests that, within the explored range, model performance is only weakly sensitive to the spatial context defined by patch size. For tree cover, performance remains largely stable across patch sizes, with only minor variations, indicating robustness to the choice of spatial context.

B.5 Compute Time

We report average training time across seeds for all models evaluated in the main experiments and ablations. All models are trained on a single GPU (NVIDIA H200) under identical settings.

Among segmentation models, MiT-B3 requires ~ 8 h for patch size 640 and ~ 7 h for 512 and ~ 7 h for 224. MiT-B1 requires ~ 4 h. U-Net variants (ResNet-34 and ResNet-50) require ~ 5 h, while DeepLabV3+ requires ~ 4 h (ResNet-34) and ~ 5 h (ResNet-50). Mask2Former is more computationally intensive, requiring ~ 23 h (Tiny) and ~ 25 h (Small).

Foundation-based models converge faster. DINOv2-B requires ~ 7 h in the single-layer setting, while multi-layer variant requires ~ 8 h (Base).

Table 4: Ablation study on model parameters. We report aggregated F1 for biome groups and resolutions. Results are averaged over multiple seeds, with twice the standard deviation ($\pm 2\sigma$) shown in parentheses. Best results are highlighted in **bold**.

Model	Patch Size	Temp.	Tropical	Boreal	Drylands	5cm	10cm	20cm
Mortality (F1)								
MiT-B3 (dice)	640	0.53 (± 0.04)	0.66 (± 0.02)	0.57 (± 0.03)	0.56 (± 0.02)	0.58 (± 0.01)	0.54 (± 0.03)	0.43 (± 0.04)
MiT-B3	640	0.58 (± 0.04)	0.66 (± 0.00)	0.58 (± 0.01)	0.56 (± 0.04)	0.60 (± 0.03)	0.55 (± 0.02)	0.45 (± 0.01)
MiT-B3	512	0.55 (± 0.05)	0.66 (± 0.00)	0.58 (± 0.02)	0.56 (± 0.01)	0.59 (± 0.03)	0.54 (± 0.01)	0.44 (± 0.03)
MiT-B3	224	0.55 (± 0.07)	0.67 (± 0.01)	0.53 (± 0.03)	0.58 (± 0.01)	0.59 (± 0.04)	0.54 (± 0.01)	0.43 (± 0.03)
Tree cover (F1)								
MiT-B3 (dice)	640	0.84 (± 0.01)	0.91 (± 0.01)	0.93 (± 0.00)	0.92 (± 0.00)	0.89 (± 0.00)	0.89 (± 0.00)	0.89 (± 0.00)
MiT-B3	640	0.85 (± 0.01)	0.92 (± 0.00)	0.93 (± 0.00)	0.93 (± 0.00)	0.89 (± 0.00)	0.89 (± 0.00)	0.89 (± 0.00)
MiT-B3	512	0.85 (± 0.01)	0.92 (± 0.01)	0.93 (± 0.00)	0.92 (± 0.00)	0.89 (± 0.00)	0.90 (± 0.01)	0.89 (± 0.01)
MiT-B3	224	0.86 (± 0.03)	0.91 (± 0.02)	0.93 (± 0.01)	0.92 (± 0.00)	0.90 (± 0.02)	0.90 (± 0.02)	0.88 (± 0.01)

Overall, training time scales with model capacity and architectural complexity, with transformer-based segmentation models incurring higher compute cost compared to lighter or frozen-backbone approaches.